Decay of Batchelor and Saffman rotating turbulence

Tomas Teitelbaum[1] and Pablo D. Mininni[1,2]

[1]*Departamento de Física, Facultad de Ciencias Exactas y Naturales, Universidad de Buenos Aires, and IFIBA, CONICET, Ciudad Universitaria, 1428 Buenos Aires, Argentina*

[2]*NCAR, P.O. Box 3000, Boulder, Colorado 80307-3000, USA*

The decay rate of isotropic and homogeneous turbulence is known to be affected by the large-scale spectrum of the initial perturbations, associated with at least two canonical self-preserving solutions of the von Kármán–Howarth equation: the so-called Batchelor and Saffman spectra. The effect of long-range correlations in the decay of anisotropic flows is less clear, and recently it has been proposed that the decay rate of rotating turbulence may be independent of the large-scale spectrum of the initial perturbations. We analyze numerical simulations of freely decaying rotating turbulence with initial energy spectra $\sim k^4$ (Batchelor turbulence) and $\sim k^2$ (Saffman turbulence) and show that, while a self-similar decay can not be identified for the total energy, the decay is indeed affected by long-range correlations. The decay of two- and three-dimensional modes follows distinct power laws in each case, which are consistent with predictions derived from the anisotropic von Kármán–Howarth equation, and with conservation of anisotropic integral quantities by the flow evolution.

I. INTRODUCTION

Turbulent flows subject to background rotation are an important problem in fluid mechanics as several systems are affected by rotation. Rotation affects the Earth's atmosphere and the oceans at large scales, it is crucial in many engineering flows such as in turbomachinery, and is also important in many astrophysical systems such as stellar convective regions and gaseous planet atmospheres. As many applications arise in nature and technology, it becomes important to understand detailed properties of these flows.

In particular, a long-lasting problem in fluid mechanics is that of the decay of turbulent fluctuations. The rate of energy decay in turbulent flows is known to be sensitive to initial conditions, and no single universal solution to the decay appears to exist to which all flows converge asymptotically for infinite Reynolds number [1]. Considering isotropic and homogeneous turbulence at high Reynolds number, there are two well known canonical cases as far as the energy spectrum at large scales is concerned. Provided the cubic velocity correlation tensor $\langle u_i(\mathbf{x})u_j(\mathbf{x})u_k(\mathbf{x} + \mathbf{r})\rangle$ decays sufficiently fast for large r, these cases correspond to the so-called Saffman spectrum for which $E(k \to 0) \sim Lk^2$, and to the so-called Batchelor spectrum where $E(k \to 0) \sim Ik^4$. Which of these spectra is observed depends on the initial conditions, and other noncanonical cases may arise if the above condition on the decay of the correlation tensor does not hold (see, e.g., [2]). The quantities L and I are approximately conserved integrals for fully developed, freely decaying turbulence in each case (I is often called the Loitsyansky integral), and have been used to determine the decay rate of the total energy (see [3–6] for examples). The quasiconservation in each case is associated with self-preserving solutions of the von Kármán–Howarth equations, and can also be interpreted in terms of conservation of linear and angular momentum. While constancy of L is a consequence of linear momentum conservation [5], constancy of I is a consequence of the conservation of angular momentum [7,8].

The presence of background rotation breaks down isotropy as a preferred direction arises along the axis of rotation (for detailed studies of rotating turbulence, see [9–11]). Flows subjected to rotation develop anisotropies which have been shown to impact dramatically on the decay of energy, and there are different and sometimes conflicting results in the literature regarding the decay laws followed by the energy in rotating flows. Moreover, theoretical arguments based on the isotropic von Kármán–Howarth equations are not valid anymore, and must be extended to include the effect of rotation. The integrals I and L become tensors, and for axisymmetric flows, some of the diagonal components of these tensors can be expected to replace I and L as approximately conserved quantities. Extensions of these arguments to anisotropic cases such as conducting flows with an imposed magnetic field, rotating, or stratified flows, have been recently derived in Refs. [7,12,13].

The development of anisotropies in rotating flows has been reported both in experiments and simulations. Experiments of freely decaying rotating turbulence show a reduction of the energy transfer, evidenced by a decrease in the energy decay rate. In the seminal experimental work using rotating grid turbulence in Ref. [14], a slowdown of the energy decay together with an anisotropic growth of the length scales parallel and perpendicular to the rotation axis for increasing rotation rates was reported. Also, a rotation dominated regime was characterized based on macroscopic Rossby numbers. The anisotropic growth of characteristic length scales was also reported in Ref. [15], although in experiments that are locally forced. An anisotropic energy flux with a trend towards quasi-two-dimensionalization has been recently reported [16], and is also evidenced, e.g., by a confirmation of the increase in the correlation lengths along the axis of rotation [17,18]. Regarding the energy decay, experimental results for nonrotating grid turbulence with integral scales smaller than the size of the vessel [19] show an energy decay $E \sim t^{-1.1}$ compatible with the theoretical result $E \sim t^{-6/5}$ expected for large-scale initial conditions with Saffman spectrum $\sim k^2$. In Ref. [20], a transition from a $E \sim t^{-6/5}$ decay to a decay

law closer to $\sim t^{-3/5}$ is reported once rotation starts affecting the flow dynamics, together with a cyclone-anticyclone asymmetry evidenced by positive skewness which grows with rotation rate. The decay for bounded flows, in which initial integral scales are close to the size of the vessel, seems to change from $E \sim t^{-2}$ to $\sim t^{-1}$ when rotation is present [19].

Numerical simulations and models also show a slowdown of the energy decay for many different initial conditions [11,21–24], together with the trend towards two dimensionalization [22,25], and the higher cyclonic-over-anticyclonic activity [26,27]. The first theoretical study of the decay of rotating turbulence was reported in Ref. [28], and considered the decrease of the energy transfer in the presence of rotation to explain the observed slowdown in the decay, and to predict decay rates for the energy. The exponents reported were consistent with those obtained in simulations in Ref. [14], and in the experiments in Ref. [19]. Also, a very close decay law $E \sim t^{-0.8}$ was found in Ref. [11] for a wide range of Rossby numbers (from very small to moderate values), when solving equations for inertial wave turbulence and for an eddy damped quasi-normal Markovian model (EDQNM3).

Later, in Ref. [25] a distinction was introduced between the energy contained in modes with $k_z = 0$ (E_{2D}, corresponding to two-dimensional, "slow," or "vortical" modes) and modes with $k_z \neq 0$ (E_{3D}, corresponding to three-dimensional, "fast," or "wave" modes). The authors carried a comprehensive study of the transfer of energy from 3D to 2D modes, for a wide range of Rossby numbers, and found a nonmonotonic behavior for the decay of energy for large, intermediate, and small Rossby numbers. They focused on the intermediate Rossby range, where the maximal energy transfer between 3D and 2D modes occurs (see also [29]). In this range, they reported an initial growth of E_{2D} as soon as the decay begins, that eventually results in a crossover with the monotonously decaying E_{3D}. Reference [30] also reported different behavior in the time evolution of E_{2D} and E_{3D}, but considered only the decay of the total energy $E = E_{2D} + E_{3D}$ proposing a decay that depends on the amount of background rotation $E \sim t^{-\gamma(\Omega)}$. The dependence of γ on the rotation rate was derived using phenomenological arguments resulting $\gamma \sim \Omega^{-1}$.

This variety of solutions naturally led to parametric studies of the initial condition space in numerical simulations. For nonhelical rotating flows with initial integral scale close to the size of the domain [24], a decay $E \sim t^{-1}$ was found in simulations, in agreement with the experimental results [19]. For flows with initial integral scale sufficiently smaller than the domain size, the case of initial conditions with energy spectra $\sim k^4$ was studied in detail in Refs. [26,27], where different decay rates were reported for the two- and three-dimensional modes. While E_{3D} was found to decay as in the case of isotropic turbulence, a slower decay was found for E_{2D} in the intermediate-Rossby range as defined in Ref. [25]. The decay of two-dimensional modes can be correctly explained if only a few components of the Loytsiansky tensor are considered (here referred in short as $I_\perp$ and $I_\parallel$ based on the symmetries of the flow), and it was shown that $I_\perp$ remains approximately constant during the decay [27]. Finally, it was also found that the decay is influenced by the amount of total helicity present in the initial conditions, and by the initial degree of anisotropy in the flow.

Recently, the anisotropic von Kármán–Howarth equation was used to consider the decay of a rotating turbulent flow with initial conditions following a Saffman spectrum [12]. The approximately conserved integral L in the isotropic and homogeneous cases was generalized in the axisymmetric case to two integrals $L_\perp \propto L_{xx} = L_{yy}$ and $L_\parallel = L_{zz}$. Assuming that both $L_\perp$ and $L_\parallel$ are simultaneously conserved (or $I_\perp$ and $I_\parallel$ for the case of Batchelor initial spectrum), and using the empirical result that characteristic length scales of the flow in the direction parallel to the rotation axis grow linearly with time [12], the author concludes that regardless of the initial spectrum being $\sim k^2$ or $\sim k^4$, both cases should decay with the same $E \sim t^{-1}$ law, thus implying that it is not possible to set apart $\sim k^2$ from $\sim k^4$ turbulence by measuring the energy decay exponent alone.

In this paper, we analyze whether the decay of rotating flows is affected by long-range correlations, studying the energy decay rate for flows with $\sim k^2$ and $\sim k^4$ initial conditions. We first present a brief theoretical discussion of conserved integral quantities for rotating turbulence using a von Kármán–Howarth equation which includes a Coriolis term due to rotation. We extend the previously derived results for Saffman turbulence [12], considering Batchelor spectrum. The results corroborate the phenomenological arguments used in Ref. [27] to explain the decay laws found numerically for energy spectra k^4. In the second part of the paper, we use numerical simulations to analyze the decay of rotating Saffman and Batchelor turbulence in periodic domains. We focus on the regime of intermediate Rossby numbers (initial Ro ≈ 0.1 [25]), and therefore we will not attempt a study of the dependence of the decay with the rotation rate. To the best of our knowledge, the free decay of energy for $\sim k^2$ initial conditions has not yet been numerically studied for rotating turbulence, and the resulting decay laws seem to be relevant for experiments. We show that the decay of energy in two- and three-dimensional modes follows distinct power laws for the cases of Batchelor and Saffman turbulence. The decay laws are consistent with the predictions derived from the anisotropic von Kármán–Howarth equation, and with the approximate constancy of either $L_\perp$ or $I_\perp$ as the flow decays.

II. VON KÁRMÁN–HOWARTH EQUATIONS AND SELF-SIMILAR DECAY

The dynamics of an incompressible fluid subjected to background rotation is described by the Navier-Stokes equation with the addition of the Coriolis acceleration,

$$\partial_t \mathbf{u} + \boldsymbol{\omega} \times \mathbf{u} + 2\boldsymbol{\Omega} \times \mathbf{u} = -\nabla \mathcal{P} + \nu \nabla^2 \mathbf{u}, \quad (1)$$

together with the incompressibility condition

$$\nabla \cdot \mathbf{u} = 0. \quad (2)$$

Here, $\mathbf{u}$ is the velocity field, $\boldsymbol{\omega} = \nabla \times \mathbf{u}$ is the vorticity, the centrifugal acceleration is absorbed in the total pressure per unit of mass $\mathcal{P}$, and ν is the kinematic viscosity. We assume uniform density and the rotation axis in the z direction so $\boldsymbol{\Omega} = \Omega \hat{z}$, with Ω the rotation frequency.

We briefly present the derivation of the von Kármán–Howarth equation including the Coriolis term in order to find invariant quantities during the self-similar energy decay in

rotating flows. To this end, we write the Navier-Stokes equation in a rotating frame in index notation, and evaluated at two points $\mathbf{x}$ and $\mathbf{x}' = \mathbf{x} + \mathbf{r}$,

$$\frac{\partial u_i}{\partial t} = -\frac{\partial}{\partial x_k}(u_i u_k) - \frac{\partial p}{\partial x_i} + \nu \nabla^2 u_i - 2\epsilon_{imn}\Omega_m u_n \quad (3)$$

and

$$\frac{\partial u_j'}{\partial t} = -\frac{\partial}{\partial x_k'}(u_j' u_k') - \frac{\partial p'}{\partial x_j'} + \nu \nabla'^2 u_j' - 2\epsilon_{jmn}\Omega_m u_n', \quad (4)$$

where $\mathbf{u}' = \mathbf{u}(\mathbf{x}')$, ∇'^2 denotes Laplacian with respect to the $\mathbf{x}'$ coordinate, and ϵ is the Levi-Civita symbol. Multiplying Eq. (3) by u_j', Eq. (4) by u_i, summing and averaging, we get the equation for the time evolution of the two-point velocity correlation tensor

$$\frac{\partial}{\partial t}\langle u_i u_j' \rangle = -\left(\frac{\partial}{\partial x_k}\langle u_j' u_i u_k \rangle + \frac{\partial}{\partial x_k'}\langle u_i u_j' u_k' \rangle \right)$$
$$- \left(\frac{\partial}{\partial x_i}\langle u_j' p \rangle + \frac{\partial}{\partial x_j'}\langle u_i p' \rangle \right) + \nu(\nabla^2 \langle u_j' u_i \rangle.$$
$$+ \nabla'^2 \langle u_i u_j' \rangle) - 2\Omega_m \langle \epsilon_{imn} u_n u_j' + \epsilon_{jmn} u_n' u_i \rangle. \quad (5)$$

If $\Omega = 0$, and assuming the cubic velocity correlation tensor $\langle u_i u_j u_k' \rangle$ and the pressure-velocity correlation $\langle u_i p' \rangle$ decay fast enough with r when $r \to \infty$, two possible integral conserved quantities can be obtained from Eq. (5). When the terms on the right-hand side of the equation go to zero as $O(r^{-2})$, then it follows from the time derivative on the left-hand side that

$$L = \int \langle \mathbf{u} \cdot \mathbf{u}' \rangle d\mathbf{r} \quad (6)$$

is conserved. This is know as the Saffman integral [5]. Multiplying Eq. (5) by r^2, another possible invariant is obtained when the terms on the left-hand side are $O(r^{-4})$, namely,

$$I = -\int r^2 \langle \mathbf{u} \cdot \mathbf{u}' \rangle d\mathbf{r}, \quad (7)$$

which is known as the Loitsyanski integral and whether it actually remains constant or not in decaying isotropic and homogeneous turbulence has been a matter of debate [31]. As the energy spectrum for small values of k can be expanded as

$$E(k \to 0) \sim Lk^2 + Ik^4 + \cdots, \quad (8)$$

the integrals L or I are then expected to be quasi-invariants during the decay for initial large-scale energy spectra of the form $\sim k^2$ (Saffman spectrum) [5,6] or $\sim k^4$ (Batchelor spectrum) [4], respectively. Using these quasiconserved integrals, the energy balance equation $dE/dt \sim -E^{3/2}/l$ can be closed (as either $l^3 u^2$ or $l^5 u^2$ are constant, with l the energy-containing scale), and different decay laws arise for each scaling of the initial spectra:

$$E(t) \sim \begin{cases} t^{-6/5} & \text{if} \quad E(k, t=0) \sim k^2, \\ t^{-10/7} & \text{if} \quad E(k, t=0) \sim k^4. \end{cases} \quad (9)$$

These decay laws have been observed in numerical as well as in experimental studies (see, e.g., [3,5,6,19,20,27,32]).

These isotropic integrals have been also assumed to remain constant during the decay of rotating turbulence with $\sim k^2$ and $\sim k^4$ large-scale energy spectra to predict energy decay laws [28]. In the presence of rotation, the energy per unit of time (flux) transferred towards smaller scales is reduced as Ω is increased. A phenomenological expression consistent with the observations is to assume that the flux is reduced by the ratio of the turnover time $\tau \sim l/E^{1/2}$ to the wave time $(2\Omega)^{-1}$ [22,33–35], resulting in Ref. [28]

$$\frac{dE}{dt} \sim -\frac{E^2}{\Omega l^2}. \quad (10)$$

Further assuming I or L are conserved results in the following decays:

$$E(t) \sim \begin{cases} t^{-3/5} & \text{if} \quad E(k, t=0) \sim k^2, \\ t^{-5/7} & \text{if} \quad E(k, t=0) \sim k^4. \end{cases} \quad (11)$$

Although these power laws are close to the behavior found in experiments and simulations, as mentioned in the Introduction, a better agreement with observations can be obtained when the arguments are extended to consider the effect of anisotropy in the flow.

In the anisotropic case, and assuming absence of long-range correlations, only the final term in Eq. (5) can contribute to the rate of change of integrals of the type

$$I_{ijmn} = \int r_m r_n \langle u_i u_j' \rangle d\mathbf{r} \quad (12)$$

for the Batchelor case, or

$$L_{ij} = \int \langle u_i u_j' \rangle d\mathbf{r} \quad (13)$$

for Saffman turbulence. It is important to point out here that it is not trivial that in this case long-range correlations should vanish as in the isotropic case [especially for the pressure velocity correlations, see [11] where these terms are computed using the Fourier transform of Eq. (5) and the Poisson equation for the pressure fluctuations]. Thus, the validity of the assumptions can only be verified *a posteriori* from the results obtained from the numerical simulations.

Assuming long-range correlations vanish sufficiently fast at large scales, the problem is that of finding which components of the tensors in Eqs. (12) and (13) are still conserved in the presence of rotation. We derive here the Batchelor case (I_{ijmn}) under the same assumptions for the decay of velocity correlations with r as in the isotropic case, multiplying Eq. (5) by $r_m r_n$ and integrating to obtain

$$\frac{\partial}{\partial t}\int r_m r_n \langle u_i u_j' \rangle d\mathbf{r}$$
$$= -2\Omega_l \int r_m r_n (\epsilon_{ilk}\langle u_k u_j' \rangle + \epsilon_{jlk}\langle u_k' u_i \rangle) d\mathbf{r}. \quad (14)$$

Let us assume $\Omega_l = \Omega_z \delta_{lz}$, so

$$\frac{\partial}{\partial t}\int r_m r_n \langle u_i u_j' \rangle d\mathbf{r}$$
$$= -2\Omega_z \int r_m r_n (\epsilon_{izk}\langle u_k u_j' \rangle + \epsilon_{jzk}\langle u_k' u_i \rangle) d\mathbf{r}. \quad (15)$$

As the flow has axisymmetry, we are interested in the diagonal components of the tensor. For $j = i$,

$$\Omega_z \epsilon_{izk} \langle u_k u_i' \rangle = \Omega_z \langle u_x u_y' - u_y u_x' \rangle, \tag{16}$$

$$\Omega_z \epsilon_{jzk} \langle u_k' u_j \rangle = \Omega_z \langle u_x' u_y - u_y' u_x \rangle, \tag{17}$$

where all terms with $i = z$ or $j = z$ vanish. For $m = n$, introducing $\mathbf{r}_\perp = (r_x, r_y, 0)$ and $\mathbf{u}_\perp = (u_x, u_y, 0)$ we get

$$\frac{\partial}{\partial t} \int r_\perp^2 \langle u_\perp u_\perp' \rangle d\mathbf{r}$$
$$= -2 \int r_\perp^2 \Omega_z [\langle u_x u_y' - u_y u_x' \rangle - \langle u_x u_y' - u_y u_x' \rangle] d\mathbf{r}, \tag{18}$$

so the terms on the right-hand side of the equation cancel and

$$\frac{\partial}{\partial t} \int r_\perp^2 \langle \mathbf{u}_\perp \mathbf{u}_\perp' \rangle d\mathbf{r} = 0 \tag{19}$$

or, equivalently,

$$I_\perp = \int r_\perp^2 \langle \mathbf{u}_\perp \mathbf{u}_\perp' \rangle d\mathbf{r} = \text{const.} \tag{20}$$

The case of Saffman turbulence was considered in Ref. [12]. The relevant components of the tensor L_{ij} for axisymmetric flows are $L_{xx} = L_{yy}$ and L_{zz}. Similar arguments as those described above lead, for the xx and yy components of the von Kármán–Howarth equation, to the conservation of the integral

$$L_\perp = \int \langle \mathbf{u}_\perp \mathbf{u}_\perp' \rangle d\mathbf{r} = \text{const.} \tag{21}$$

Note that both $I_\perp$ and $L_\perp$ resemble integrals that arise in the context of the decay of 2D turbulence [36]. This is to be expected as the spectrum of an axisymmetric flow can be expanded, for the modes with $k_\parallel = k_z = 0$, as

$$E(k_\perp \to 0, k_\parallel = 0) \approx L_\perp k_\perp + I_\perp k_\perp^3 + \cdots, \tag{22}$$

which is (except for differences in the dimensions) also the expansion of a 2D energy spectra. The resemblance can be expected as rotating flows tend to become quasi-2D, concentrating most of the energy in the slow modes with $k_\parallel = 0$.

For axisymmetric turbulence and a Batchelor initial spectrum $\sim k^4$ at large scales, Eq. (20) leads to

$$I_\perp \sim l_\perp^4 l_\parallel u_\perp^2 \approx \text{const,} \tag{23}$$

where $l_\perp$ and $l_\parallel$ are characteristic (energy-containing) scales in the perpendicular and parallel directions, respectively. Assuming 2D and 3D modes are only weakly coupled in rotating turbulence, from Eq. (10) we can write an equation for the decay of the energy in 2D modes

$$\frac{dE_{2D}}{dt} \sim -\frac{E_{2D}^2}{\Omega I_\perp^2}, \tag{24}$$

and from Eq. (23)

$$\frac{dE_{2D}}{dt} \sim -\frac{E_{2D}^{5/2} l_\parallel^{1/2}}{I_\perp^{1/2} \Omega}. \tag{25}$$

Assuming $E_{2D} \sim t^\gamma$, it follows that [27]

$$E_{2D} \sim t^{-2/3} \tag{26}$$

if $l_\parallel$ remains constant (which is reasonable as 2D modes have no dependence on the direction parallel to rotation, and therefore $l_\parallel = l_0$ is the vertical size of the box).

For a $\sim k^2$ initial spectra,

$$L_\perp \sim l_\perp^2 l_\parallel u_\perp^2 \approx \text{const,} \tag{27}$$

and replacing in Eq. (24) leads to

$$\frac{dE_{2D}}{dt} \sim -\frac{E_{2D}^3 l_\parallel}{L_\perp \Omega}, \tag{28}$$

and a decay

$$E_{2D} \sim t^{-1/2}. \tag{29}$$

The results for the decay of energy in 2D modes in rotating turbulence can be summarized as follows:

$$E_{2D}(t) \sim \begin{cases} t^{-1/2} & \text{if } E(k, t = 0) \sim k^2, \\ t^{-2/3} & \text{if } E(k, t = 0) \sim k^4. \end{cases} \tag{30}$$

It is worth mentioning that the decay of rotating turbulence with $\sim k^2$ spectra is discussed in detail in Ref. [12], where the constancy of $L_\perp$ is obtained from the von Kármán–Howarth equation. In that case, the author also considers the von Kármán–Howarth equation for the zz component of the two-point correlation tensor, and assuming cubic correlations decay fast enough also for that component, obtains constancy of $L_\parallel \sim u_\parallel^2 l_\perp^2 l_\parallel$ as well as of $L_\perp$. The constancy of these two quantities, together with the empirical result $l_\parallel = l_0(1 + \kappa \Omega t)$ (where κ is a constant of order one [14,17]) leads to a decay $E_{2D}(t) \sim t^{-1}$. A similar argument for Batchelor $\sim k^4$ turbulence leads to the same decay, which would result in an impossibility to distinguish between $\sim k^2$ and $\sim k^4$ turbulence by measuring the energy decay exponent alone.

Finally, it is interesting to point out that constancy of $I_\perp$ and $L_\perp$ can be respectively associated with conservation of the z component of angular and linear momentum (see [7,12]). In fact, the mean squared angular momentum H_z averaged over a cylinder-shaped volume V is

$$\langle H_z^2 \rangle = 2\pi V l_\parallel I_\perp, \tag{31}$$

while the linear momentum P_z is

$$\langle L_z^2 \rangle = 2\pi V l_\parallel L_\perp. \tag{32}$$

III. NUMERICAL SIMULATIONS

In the following, we resort to numerical simulations to verify the validity of the assumptions and predictions discussed in the previous section. As a well resolved initial spectrum $\sim k^2$ or $\sim k^4$ is needed to observe constancy of I or L in simulations of isotropic and homogeneous turbulence (see, e.g., [3]), we use large-eddy simulations (LES) in periodic boxes to be able to have initial energy containing wave number $k_0 \approx 40$ with large Reynolds numbers at a reasonable computing cost.

Before proceeding, we must caution the reader on how the simulations in periodic boxes should be interpreted. Flows

in periodic boxes are sometimes considered as describing a homogeneous flow in an infinitely periodic domain. In this work, we will interpret instead a flow in a periodic box as artificially confined. Indeed, as was shown in Ref. [27], when the integral scale of the flow is close to the domain size, the eddies can not become larger and the energy decay laws obtained are those of confined flows. The confinement is artificial in the sense that the flows have no Ekman layers, as the domain has no rigid walls. Moreover, the confinement also results in a discrete set of wave numbers and selects a discrete set of inertial waves which are normal modes of the domain, unlike homogeneous rotating flows in infinite domains which have continuous wave numbers (see, e.g., [11,37]). Note that due to the discretization of wave numbers in the former case, the existence and number of exact resonances depend on the domain size [37] (as this is aggravated when boxes with large aspect ratio and lower resolution in the vertical direction are used, we restrict our study to boxes with aspect ratio of unity).

While these are unavoidable and inherent properties of the simulations in periodic domains, the choice of a relatively large initial energy containing wave number $k_0 \approx 40$ ensures that as the equations are advanced in time, the energy containing scale of the flow will remain smaller than the box size, and that a large fraction of wave numbers will be available at large scales for the system to evolve.

A. Equations and model

Equations (1) and (2) are solved numerically using a dynamical subgrid-scale spectral LES model of rotating turbulence in which only the large scales are explicitly resolved. The statistical effect of unresolved scales on the scales larger than a cutoff wave number ($k_c = N/2$) are modeled with an eddy viscosity and eddy noise that are obtained after solving in each time step the eddy damped quasi-normal Markovian (EDQNM) equations for the spectrum of the unresolved scales. Details of the LES can be found in Ref. [38], and in Refs. [39,40] for its extension to the rotating case. A validation of the LES against direct numerical simulations (DNS) for the case of freely decaying rotating turbulence can be found in Ref. [27].

The simulation domain is a 3D periodic box of length 2π with spatial resolution of 256^3 grid points (resulting in $k_c = 128$). A parallelized pseudospectral method without dealiasing is used to solve spatial derivatives, and an explicit second-order Runge-Kutta method is used to evolve in time [41].

B. Initial conditions

In Ref. [27], it was observed that the energy decay is sensitive to the initial anisotropy of the flow (in particular, to the initial amount of energy in 2D modes). To enforce spectral and variance isotropy of the initial conditions, we generate at $t = 0$ a random velocity field using the Craya-Herring decomposition [42,43] which associates to each wave vector $\mathbf{k}$ an orthonormal frame with axes dependent on $\mathbf{k}$ as

$$\mathbf{i}(\mathbf{k}) = \frac{\mathbf{k} \times \alpha}{|\mathbf{k} \times \alpha|}, \quad \mathbf{j}(\mathbf{k}) = \frac{\mathbf{k} \times \mathbf{i}}{|\mathbf{k}|}, \quad \frac{\mathbf{k}}{k}; \quad (33)$$

α is an arbitrary but fixed unit vector which we choose to be parallel to the rotation axis, $\alpha = (0,0,1)$. This representation

has been widely used to study turbulence (see, e.g., [44,45]). Random initial conditions are created through a superposition of harmonic modes with random phases $\phi(\mathbf{k}), \phi'(\mathbf{k})$ projected over the Craya reference system for each $\mathbf{k}$,

$$\mathbf{u}(\mathbf{k}) = e^{i\phi}\mathbf{i} + e^{i\phi'}\mathbf{j}. \quad (34)$$

Note that due to the geometry of the Craya-Herring decomposition, there is no projection of $\mathbf{u}$ into $\mathbf{k}$ as the incompressibility condition stands for $\mathbf{u}(\mathbf{k}) \perp \mathbf{k}$.

As we are interested in the decay laws followed by flows with a particular initial spectrum (either Batchelor's or Saffman's), we can further control the shape of the initial isotropic spectrum by multiplying each mode $\mathbf{u}(\mathbf{k})$ in Fourier space with $0 < k \leqslant k_0$ by an amplitude Ck^β, where C is a constant to get initial root-mean-square (rms) velocity $U \approx 1$, and β is a parameter used to adjust the power law in $E(k)$. For $k > k_0$, the spectrum is continued by an exponential decay up to k_c (the maximum wave number explicitly resolved in the simulations).

C. Spectra

In order to characterize the simulations, we consider isotropic as well as anisotropic spectra. The latter are useful to analyze rotating flows in which anisotropies grow with time. In the simulations, the isotropic spectrum is defined by averaging in Fourier space over spherical shells,

$$E(k,t) = \frac{1}{2} \sum_{k \leqslant |\mathbf{k}| < k+1} \mathbf{u}^*(\mathbf{k},t) \cdot \mathbf{u}(\mathbf{k},t), \quad (35)$$

where the asterisk denotes complex conjugate. For the anisotropic spectrum, the components of $\mathbf{u}(\mathbf{k})$ are integrated around the axis of rotation to obtain a spectrum that depends only on $k_\perp$,

$$E(k_\perp) = \frac{1}{2} \sum_{k_\perp \leqslant |\mathbf{k}_\perp| < k_\perp+1} \mathbf{u}^*(\mathbf{k},t) \cdot \mathbf{u}(\mathbf{k},t). \quad (36)$$

From now on, we will reference these two spectra simply as $E(k)$ and $E(k_\perp)$, respectively.

More detailed information on the energy spectral distribution of anisotropic flows can be obtained from the axisymmetric energy spectrum $e(k_\parallel, k_\perp)$ (see, e.g., [10,45,46]). This spectrum is obtained after integrating the three-dimensional energy spectrum around the axis of rotation to obtain a spectrum that depends only on $k_\parallel$ and $k_\perp$, and that relates to $E(k_\perp)$ as follows:

$$E(k_\perp) = \sum_{k_\parallel} e(k_\parallel, k_\perp). \quad (37)$$

Finally, the spectrum of the initial conditions is such that the Saffman or Batchelor power laws $\sim k^2$ or $\sim k^4$ are imposed in $E(k)$. The relationship between the power law in $E(k)$ and of that of $E(k_\perp)$ can be derived as follows. Equation (35) in the continuous limit can be expressed as

$$E(k,t) = \frac{1}{2} \int \hat{\Phi}_{ii}(k,t)k^2 d\Omega_k, \quad (38)$$

where $\hat{\Phi}_{ij}$ is the spectral tensor, i.e., the Fourier transform of the second-order velocity correlation function

$\Phi_{ij} \langle u_i(\mathbf{x},t)u_j(\mathbf{x}+\mathbf{r},t)\rangle$, and where Ω_k is the solid angle in Fourier space. Per virtue of Eq. (38), if $E(k,0) \sim k^\sigma$, then $\hat{\Phi}_{ii} \sim k^{\sigma-2}$. For axisymmetric flows we can write the energy spectrum $E(k_\perp)$ integrating in complex space over cylindrical shells,

$$E(k_\perp,t) = \frac{1}{2} \int \hat{\Phi}_{ii}(k_\perp,t)k_\perp d\phi_k dk_z. \tag{39}$$

If $E(k,0) \sim k^\sigma$, then

$$\begin{aligned} E(k_\perp,0) &= \frac{1}{2} \int k^{\sigma-2} k_\perp d\phi_k dk_z \\ &= \frac{1}{2} \int \left(k_\perp^2 + k_z^2\right)^{\frac{\sigma-2}{2}} k_\perp d\phi_k dk_z. \end{aligned} \tag{40}$$

When most of the energy is in the $k_z = 0$ plane, then, from Eq. (40),

$$E(k_\perp,0) \sim \frac{1}{l_\parallel} \int k_\perp^{\sigma-1} d\phi_k. \tag{41}$$

Even in the case in which the energy is not concentrated in the $k_z = 0$ plane (as in the isotropic initial conditions), the dependence of $E(k_\perp)$ will be $\sim k_\perp^{\sigma-1}$ as it follows directly from Eq. (40). To summarize,

$$E(k) \sim k^\sigma \Rightarrow E(k_\perp) \sim k_\perp^{\sigma-1}. \tag{42}$$

It is important to note that this simple relation between the isotropic $E(k)$ and the anisotropic $E(k_\perp)$ spectra only holds for the isotropic initial conditions. However, the relation will be useful to understand the power laws observed at large scales in the following section. As an example, when analyzing rotating turbulence with an initial isotropic spectrum $E(k) \sim k^2$, we will be facing the case with initial $E(k_\perp) \sim k_\perp$. Note the power laws $E(k_\perp) \sim k_\perp$ and $E(k_\perp) \sim k_\perp^3$, resulting respectively for Saffman and Batchelor isotropic initial conditions, are the ones that arise in the expansion of the axisymmetric energy spectrum for $k_\parallel = 0$ and $k_\perp \to 0$ in Eq. (22).

IV. NUMERICAL RESULTS

We now present results stemming from four numerical simulations (see Table I). All runs were initialized using the random (Craya-Herring) initial conditions described in the previous section, with an initial isotropic spectrum $E(k) \sim k^2$ between $0 < k \leqslant 40$ for runs A and B, and $E(k) \sim k^4$ between $0 < k \leqslant 40$ for runs C and D. Runs A and C correspond to isotropic and homogeneous turbulence (no rotation), while runs B and D are rotating, resulting in homogeneous but

anisotropic flows as time evolves. The purpose of simulations A and C is to recover well known results for isotropic $\sim k^2$ and $\sim k^4$ turbulence, and to use them as a starting point to analyze the more complex rotating cases. Note the decay of $\sim k^4$ turbulence (corresponding to runs C and D) was studied in detail in Ref. [26], and is considered here to compare with the $\sim k^2$ case.

Parameters of the runs listed in Table I are defined as follows: The Reynolds number is

$$\mathrm{Re} = \frac{lU}{\nu}, \tag{43}$$

where U is the rms velocity and the energy-containing scale l is defined from the isotropic energy spectrum $E(k)$ as

$$l = 2\pi \frac{\int E(k)k^{-1}dk}{\int E(k)dk}. \tag{44}$$

The Reynolds number based on the Taylor scale λ is

$$\mathrm{Re}_\lambda = \frac{\lambda U}{\nu}, \tag{45}$$

where

$$\lambda = 2\pi \left(\frac{\int E(k)dk}{\int E(k)k^2dk}\right)^{1/2}. \tag{46}$$

The Rossby number is

$$\mathrm{Ro} = \frac{U}{2\Omega l}, \tag{47}$$

while the micro-Rossby number is defined as

$$\mathrm{Ro}^\omega = \frac{\omega}{2\Omega}. \tag{48}$$

This number should be initially of order one for the scrambling effect of waves not to completely damp the nonlinear term in the Navier-Stokes equation, which would result in just an exponential decay of the energy [10]. Time-dependent parameters in Table I are given for all runs at $t = 0$, and also at $t = 20$ (roughly 10 turnover times after the self-similar decay of energy starts).

A. Decay of nonrotating flows

Figure 1 shows the evolution of the isotropic energy spectrum for run A, at times ranging from $t = 0$ to 20. The initial $\sim k^2$ law is approximately preserved over time at the smallest wave numbers, while higher wave numbers decay due to the effect of dissipation. This behavior is consistent with the quasiconservation of L in Eq. (8), for which a subsequent decay law $E \sim t^{-6/5}$ is expected for the energy.

TABLE I. Parameters used in the simulations: number of linear grid points N, kinematic viscosity ν, rotation frequency Ω, Reynolds number Re, Taylor Reynolds number Re_λ, Rossby number Ro, micro-Rossby number Ro^ω, and a brief description of the initial energy spectrum $E(k)$: the power law followed at large scales and the range of scales where this power law is satisfied. Values of Re, Re_λ, Ro, and Ro_λ are given at $t = 0$, and at $t = 20$ between parentheses.

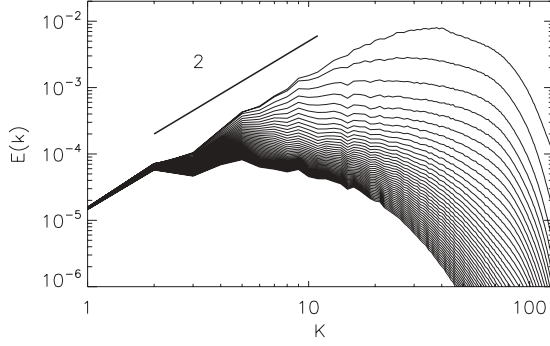| Run	N	ν	Ω	Re	Re_λ	Ro	Ro^ω	Initial $E(k)$
A	256	1.3×10^{-4}	0	1580(330)	780(100)	$\infty(\infty)$	$\infty(\infty)$	k^2 ($1 \leqslant k \leqslant 40$)
B	256	1.3×10^{-4}	33	1580(1090)	780(520)	0.15(0.004)	0.9(0.024)	k^2 ($1 \leqslant k \leqslant 40$)
C	256	1.3×10^{-4}	0	1280(150)	730(60)	$\infty(\infty)$	$\infty(\infty)$	k^4 ($1 \leqslant k \leqslant 40$)
D	256	1.3×10^{-4}	33	1280(360)	730(180)	0.18(0.002)	1.0(0.015)	k^4 ($1 \leqslant k \leqslant 40$)

FIG. 1. Evolution of the isotropic energy spectrum $E(k)$ for run A from $t = 0$ to 20 with time increments $\Delta t = 0.5$. Note how the initial $E \sim k^2$ spectrum is preserved over time at the large scales (smaller wave numbers).

Figure 2 shows the energy and enstrophy decay for runs A and C. After a transient lasting for approximately 10 turnover times, both runs decay with different power laws. In run A, the energy decays close to $E \sim t^{-6/5}$ as predicted by Eq. (9), and as expected from the shape of the large-scale spectrum in Fig. 1. The enstrophy shows a faster decay close to $Z \sim t^{-11/5}$, consistently with phenomenological arguments which indicate that $E \sim t^\alpha$ leads to $Z \sim t^{\alpha-1}$ under the assumption of isotropy, as

$$\frac{dE}{dt} = -2\nu Z(t). \quad (49)$$

The energy decay for run C is consistent with $E \sim t^{-10/7}$ as expected by Eq. (9), while the enstrophy decay is close to $Z \sim t^{-17/7}$, also consistent with Eq. (49). The spectrum of run C maintains a $\sim k^4$ shape for large scales (not shown). All these results are consistent with previous simulations and theoretical results [3,27,32].

The prediction $E \sim t^{-6/5}$ for run A assumes L remains constant during the decay. To verify this, and to further study whether L also remains constant in the decay of rotating turbulence with $\sim k^2$ spectrum, we show the time evolution of L for runs A and B in Fig. 3(a). We estimated L in two different ways: A fit to the spectrum with a power law $\sim k^2$ was computed for the smallest wave numbers to obtain the
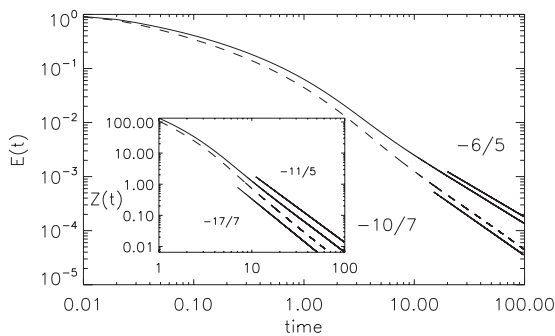

FIG. 2. Energy evolution for runs A (solid) and C (dashed). Note the decay laws with exponents $\approx -6/5$ and $\approx -10/7$, respectively, after an initial transient of ≈ 10 turnover times. Slopes are shown as a reference. Inset: enstrophy decay for the same runs. The decays approach $\approx -11/5$ and $\approx -17/7$, respectively, after $t \approx 10$.
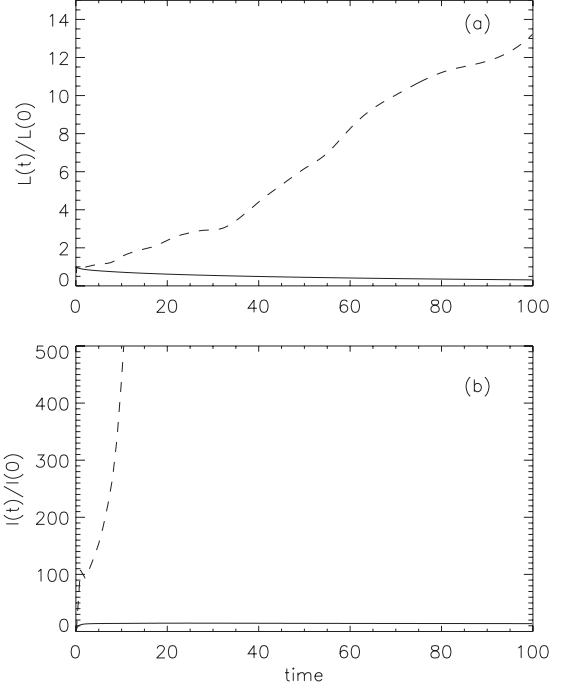

FIG. 3. (a) Evolution of the integral L normalized by its initial value $L(0)$ for the isotropic run A (solid line) and rotating run B (dashed line). (b) Evolution of the integral I normalized by its initial value $I(0)$ for the isotropic run B (solid line) and rotating run D (dashed line).

multiplicative prefactor in Eq. (8) (proportional to L if the spectrum is $\sim k^2$), as was done in Ref. [3]. We also computed the two-point correlation function from the energy spectrum using [31]

$$\langle \mathbf{u} \cdot \mathbf{u}' \rangle(r) = 2 \int_0^\infty E(k) \frac{\sin(kr) - kr\cos(kr)}{(kr)^3} dk, \quad (50)$$

and then used Eq. (6) to compute L. Both methods give consistent results and in the following we show results obtained with the last method.

In run A, L decays to half its initial value between $t = 0$ and $t \approx 10$, but after this time it only changes slowly with time and can be considered almost constant (note the energy between $t = 10$ and 100 changes by more than an order of magnitude). However, L is far from being constant in run B; the behavior of the rotating runs is discussed in more detail in the next section. Similar results were found for the evolution of I in simulations C and D, as shown in Fig. 3(b). In run C, I grows during a short transient, but stays constant during the self-similar decay of the energy.

While the behavior of L and I in the simulations is compatible with the theoretical and phenomenological arguments discussed in Sec. II, the rapid growth of these quantities in the runs with rotation seems to question the use of isotropic integrals to derive decay laws for anisotropic flows.

B. Decay of rotating flows

The analysis for runs A and C was based on the isotropic energy spectrum and on the quasi-invariance of the isotropic integrals L and I. However, the growth of L (I) in run
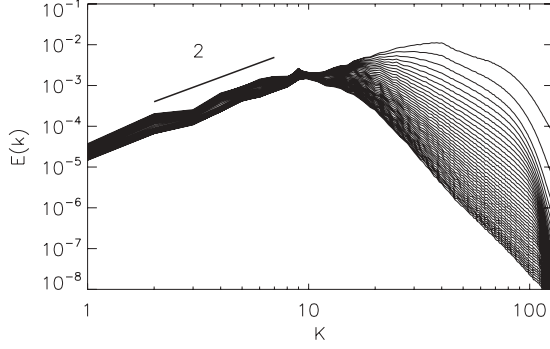
FIG. 4. Evolution of the isotropic energy spectrum $E(k)$ for run B from $t = 0$ to 20 with time increments $\Delta t = 0.5$. Note how the initial $E \sim k^2$ spectrum for large scales (low wave numbers) is preserved over time, but its overall amplitude increases.

B (D) suggests that different arguments should be used to predict their energy decay. In this light, we now consider the anisotropic quantities introduced in Sec. II, $L_\perp$ and $I_\perp$, and show that further analysis can be done by studying the evolution of anisotropic spectra and splitting the energy decay in 2D and 3D modes. A similar method was used in Ref. [27] to study $\sim k^4$ turbulence.

The evolution of the isotropic spectrum for run B is shown in Fig. 4, for different times from $t = 0$ to 20. As for run A, its initial $\sim k^2$ behavior for large scales is preserved over time. However, its amplitude at large scales increases with time, in agreement with the evolution of L.

The time evolution of the total energy in run B shows that the decay is close to, but steeper than, $E \sim t^{-3/5}$. In Fig. 5, we show the energy decay for this run (we also show the $\sim k^4$ case for comparison, i.e., run D). The decay deviates from the expected $\sim t^{-3/5}$ law derived via isotropic arguments (in the same fashion, run D deviates from the expected $\sim t^{-5/7}$ law) and strictly speaking, a power law is hard to identify. Indeed, as was shown in Fig. 3, both L and I grow fast in runs B and D. As a result, arguments based on the quasiconservation of L or I should be expected to fail to predict the correct energy decay. The reason for this failure can be associated with the fact that rotating flows are not isotropic, and instead become axisymmetric with a tendency towards two dimensionalization.
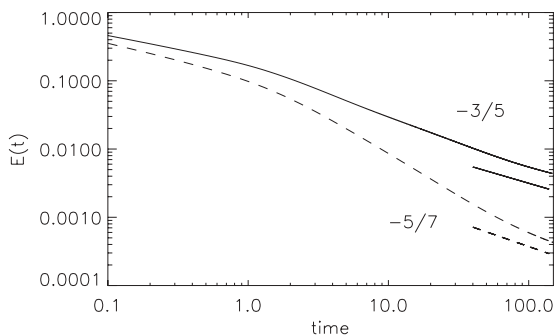

FIG. 5. Energy decay for runs B (solid line) and D (dashed line); $t^{-3/5}$ and $t^{-5/7}$ power laws are shown as a reference, corresponding to phenomenological predictions for Saffman and Batchelor rotating turbulence based on isotropic conserved quantities.
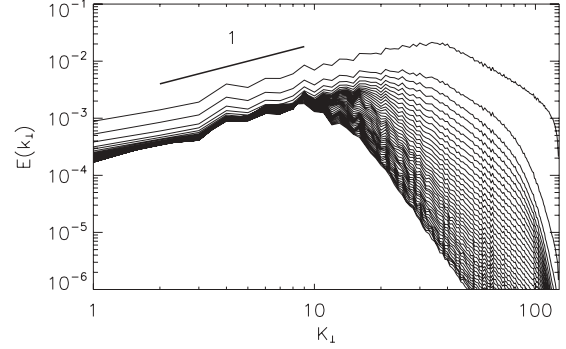

FIG. 6. Evolution of the axisymmetric energy spectrum $E(k_\perp)$ for run B from $t = 0$ to 20 with time increments $\Delta t = 0.5$. The initial shape $E \sim k_\perp$ of spectrum at large scales (low wave numbers) is approximately preserved over time.

From the arguments in Sec. II, we expect only large-scale correlations in the direction perpendicular to the axis of rotation to be preserved, and either $L_\perp$ or $I_\perp$ to remain constant depending on the initial conditions. Therefore, we analyze runs B and D with the aid of the expansion in Eq. (22) and of the anisotropic energy spectrum $E(k_\perp)$. Following Eqs. (24) and (30), we will also separate the energy into the energy of slow modes E_{2D}, and the energy of fast modes E_{3D}.

In Fig. 6, we show the time evolution of $E(k_\perp)$ in run B. Per virtue of Eq. (42), as the isotropic spectrum is $E(k) \sim k^2$ for small wave numbers, the anisotropic spectrum is $E(k_\perp) \sim k_\perp$. As for $E(k)$, the shape of the spectrum is preserved during the decay, and $E(k_\perp) \sim k_\perp$ for small $k_\perp$ at all times. However, unlike the isotropic spectrum, $E(k_\perp)$ rapidly decreases its amplitude during a short transient, and then the amplitude of the spectrum at large scales stabilizes and varies only slowly with time. Run D shows a similar behavior in $E(k)$ and $E(k_\perp)$, but following $E(k_\perp) \sim k_\perp^3$ instead.

We saw in Sec. II that constancy of $L_\perp$ ($I_\perp$) may be expected for $E(k) \sim k^2$ ($\sim k^4$) initial spectra if large-scale correlations decay fast enough, and that phenomenological analysis leads then to $E_{2D}(t) \sim t^{-1/2}$ ($E_{2D} \sim t^{-2/3}$). As for L, we estimate $L_\perp$ using two different methods: by fitting the spectrum for small $k_\perp$, and by using Eq. (21). The two-point longitudinal correlation function for the axisymmetric case is estimated using Bessel functions and the anisotropic perpendicular spectrum (see, e.g., [26,31])

$$\langle \mathbf{u}_\perp \cdot \mathbf{u}'_\perp \rangle (r_\perp) = 2 \int E(k_\perp) J_0(k_\perp r_\perp) dk_\perp. \qquad (51)$$

Both estimations give similar results and the curves discussed below are obtained from Eqs. (21) and (51). The same procedure was used to estimate $I_\perp$ from Eq. (20).

In Fig. 7, we show the evolution of $L_\perp$ and $I_\perp$ normalized by their values at $t = 0$, for runs B and D, respectively. Although at early times their values decrease rapidly, they remain afterwards approximately constant during the entire simulation (note that in the same simulations and at the same times, L and I increase by at least one order of magnitude).

The evolution of the energy for run B shows interesting properties (see Fig. 8); E_{2D} initially grows until $t \approx 10$, when it reaches its maximum value and begins to decrease. E_{3D} decreases faster than E_{2D} and at $t \approx 20$ both energies are
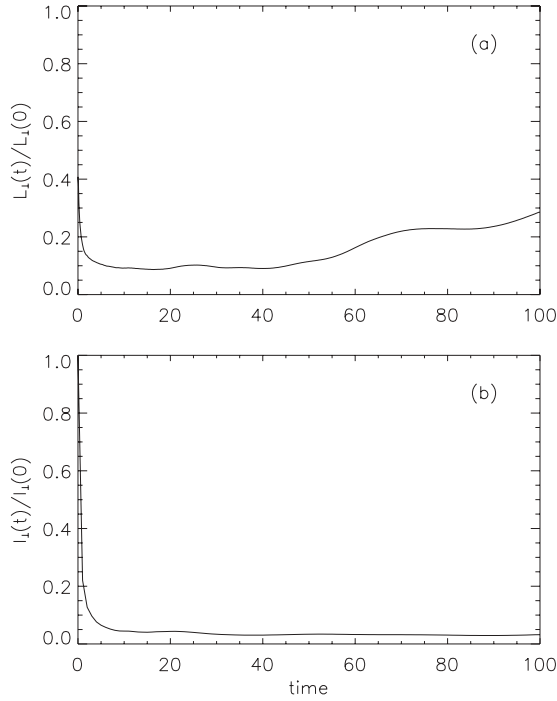
FIG. 7. (a) Ratio $L_\perp(t)/L_\perp(0)$ as a function of time for run B. (b) Evolution of $I_\perp(t)/I_\perp(0)$ in run D. Note that in both cases, these magnitudes remain approximately constant after a short initial transient.

comparable. After that time, the system is dominated by the energy in the slow modes. Starting at $t \approx 10$, both energies show a decay compatible with power laws with different exponents. $E_{2D}(t)$ decays close to $\sim t^{-1/2}$, in agreement with Eq. (30) and with the approximate constancy of $L_\perp$, while E_{3D} decays close to $\sim t^{-6/5}$, the value expected from Eq. (9) for the decay of three-dimensional Saffman turbulence.

A distinct decay of E_{2D} and E_{3D} is also observed in run D (corresponding to $\sim k^4$ turbulence, also shown in Fig. 8). The decay of the energy in slow modes is compatible with $E_{2D}(t) \sim t^{-2/3}$, as expected for Batchelor turbulence from Eq. (30) and with the approximate constancy of $I_\perp$ shown in Fig. 7. The 3D energy shows a decay that is close to $E_{3D} \sim t^{-10/7}$.

The decay of E_{2D} in runs B and D is compared in Fig. 9. The two different decay laws followed by the energy in the two runs can be clearly identified. The result indicates that the decay of rotating turbulence is affected by large-scale correlations, as different power laws can be observed for $E(k) \sim k^2$ and $\sim k^4$ initial spectra.

The different power laws followed by E_{2D} and E_{3D} after $t \approx 10$ in both runs point to a negligible interchange of energy between slow and fast modes at late times, as required for an equation such as Eq. (24) to hold. Runs B and D have initial values of the Rossby number which correspond to the intermediate Rossby range studied in Ref. [25]. In this range, maximal energy transfer from 3D to 2D modes takes place at early times, with E_{2D} in some cases growing from energy in 3D modes as a result [see Fig. 8(a)]. After this phase, the independent decay of the two energies implies that these exchanges are small compared with, e.g., the transfer of energy from vortical motions at large scales to vortical motions at
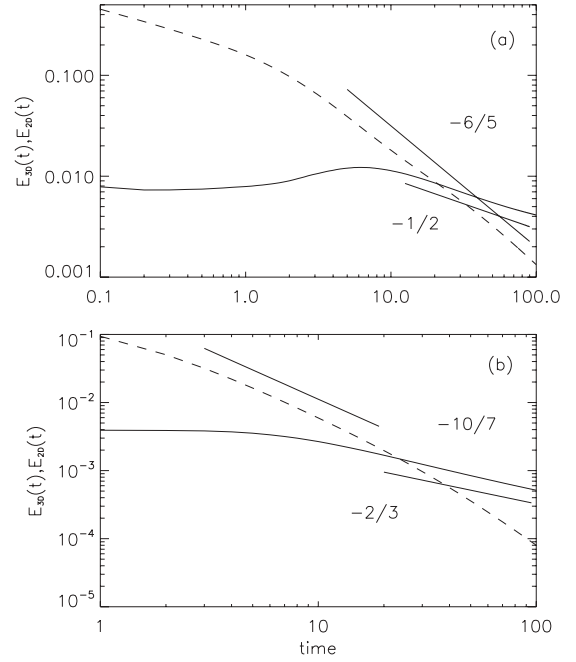

FIG. 8. (a) Time evolution of the energy E_{3D} in modes with $k_\parallel \neq 0$ (dashed line), and of the energy E_{2D} in modes with $k_\parallel = 0$, for run B. Power laws $t^{-6/5}$ and $t^{-1/2}$ are indicated as a reference, following phenomenological arguments, respectively, for the decay of the 3D energy and for the decay of the 2D energy based on approximate constancy of $L_\perp$ in Saffman turbulence. (b) Same for run D. The power laws $t^{-10/7}$ and $t^{-2/3}$ correspond to the phenomenological predictions for Batchelor turbulence.

smaller scales in E_{2D}, and the transfer from 3D modes to 3D modes in E_{3D}.

C. Energy exchange between 2D and 3D modes

A measure of the exchange of energy between 2D and 3D modes per unit of time can be obtained from the flux of energy across planes in Fourier space with normal k_z. The amount of energy per unit of time going through any of such planes is
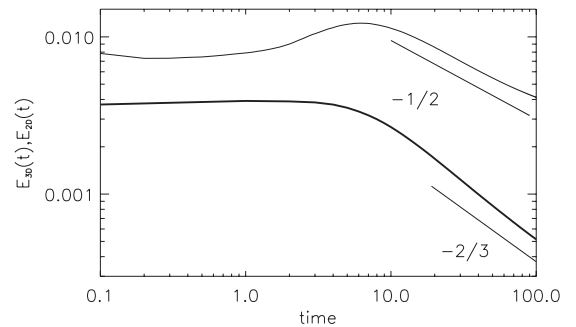

FIG. 9. E_{2D} decay as a function of time for runs B (thin line) and D (thick line). The expected decays based on constancy of $L_\perp$ and $I_\perp$ are indicated as a reference. The agreement in this case is much better than when assuming constancy of the isotropic integrals L and I (see Fig. 5).

given by

$$\Pi(k_\parallel) = -\iiint_{k_\parallel=0}^{k_\parallel} \hat{\mathbf{u}}_\mathbf{k}^* \cdot (\widehat{\mathbf{u} \cdot \nabla \mathbf{u}})_\mathbf{k} \, dk_x dk_y dk_z, \qquad (52)$$

where the integrals in k_x and k_y run over their entire range (see [47] for definitions of anisotropic fluxes and spectral transfer functions), and the hat denotes Fourier transform. The energy transferred from 2D modes to 3D modes per unit of time is then

$$S = \Pi(k_\parallel = 0). \qquad (53)$$

When S is positive, it represents transfer of energy from 2D to 3D motions (i.e., energy going from $k_\parallel = 0$ towards larger values of $k_\parallel$, resulting in an effective source of 3D energy coming from 2D loses), while when negative it represents transfer from 3D to 2D motions (i.e., a source of 2D energy from 3D loses). For these sources (or losses) of energy to be negligible, they must be small when compared with the time derivatives dE_{2D}/dt and dE_{3D}/dt. When they are, the decay of E_{2D} and of E_{3D} can be considered independently.

Figure 10 shows the function S normalized by $|dE_{2D}/dt|$ and $|dE_{3D}/dt|$ for runs B and D. In both runs S is negative before $t \approx 10$, indicating energy goes from 3D to 2D modes, and explaining the growth of E_{2D} at early times in run B. Note that in run B, $|dE_{2D}/dt|$ becomes zero at $t \approx 5$, resulting in an infinite value of the ratio $S/|dE_{2D}/dt|$ in Fig. 10(a). Later, for $t \approx 10$ in run B, and for $t \approx 20$ in run C, $S/|dE_{2D}/dt|$ and $S/|dE_{3D}/dt|$ become small, indicating the interchange of
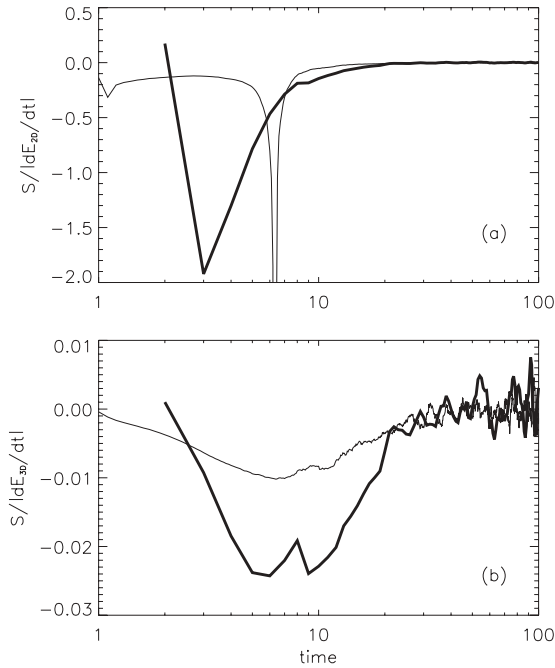
energy between slow and fast modes becomes negligible when compared with the energy decay rates, and justifying the use of separate balance equations to study the decay of E_{2D} and E_{3D}. Indeed, to have $S \ll |dE_{2D}/dt|$ and $S \ll |dE_{3D}/dt|$ is enough to consider equations for the evolution of E_{2D} and E_{3D} as was done in Sec. II, as is a more precise definition of what was meant in that section by the condition of "weakly coupled" 2D and 3D modes.

It is worth pointing out that the fact that $S/|dE_{2D}/dt|$ and $S/|dE_{3D}/dt|$ are much smaller than unity does not imply that the 2D and 3D modes are completely decoupled, and only implies that almost no energy is interchanged between slow and fast modes during the self-similar decay. Triadic interactions, e.g., between two fast modes and one slow mode, can still occur and be relevant, as long as the slow mode is only an intermediary and does not receive from nor give net energy to the fast modes. Indeed, such interactions between slow and fast modes that preserve the 2D and 3D energies separately would be required to have dE_{2D}/dt proportional to $1/\Omega$ in Eq. (25), as in their absence the decay of E_{2D} should be that of 2D Navier-Stokes and independent of Ω (note triadic interactions between three slow modes are trivially resonant and independent of Ω).

D. Energy spectral distribution

A deeper understanding of the development of anisotropy in the flow can not be obtained solely from studying the reduced spectrum $E(k_\perp)$ and the isotropic spectrum $E(k)$. To further investigate the energy spectral distribution, we present contour plots of the axisymmetric energy spectrum $e(k_\parallel, k_\perp)$ for runs A, B, and D in Figs. 11–13, respectively. Note that in order to obtain circular contour levels when the spectral distribution
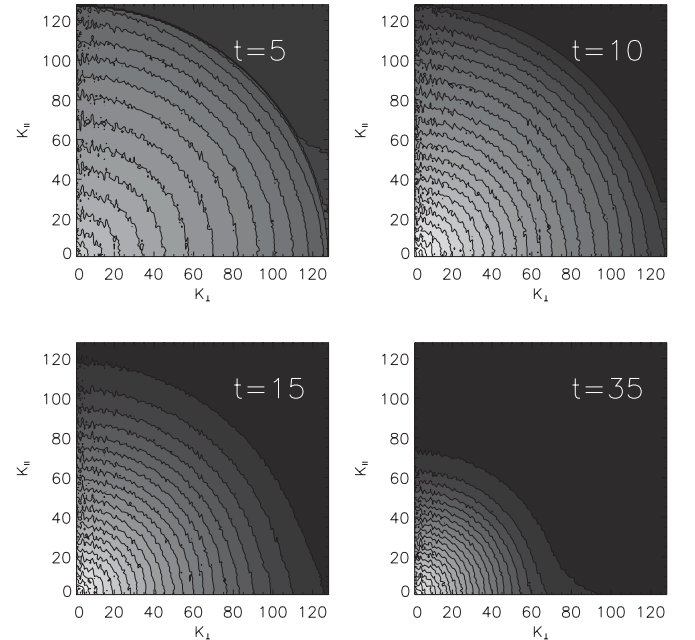

FIG. 10. (a) Energy interchanged per unit of time S between 2D and 3D modes, (a) normalized by $|dE_{2D}/dt|$ and (b) normalized by $|dE_{3D}/dt|$, for runs B (thin line) and D (thick line). Positive values of S represent flux of energy from 2D to 3D modes, while negative values indicate flux from 3D to 2D motions. At early times, S is negative, indicating energy is transferred from 3D to 2D modes. After $t \approx 10$ in run B, and $t \approx 10$ in run D, when the distinct power law decays are observed for $E_{2D}(t)$ and $E_{3D}(t)$ (Fig. 8), S becomes negligible.

FIG. 11. Axisymmetric energy spectrum $e(k_\parallel, k_\perp)/\sin\theta$ at different times in run A. The circular contour levels indicate an isotropic energy distribution.
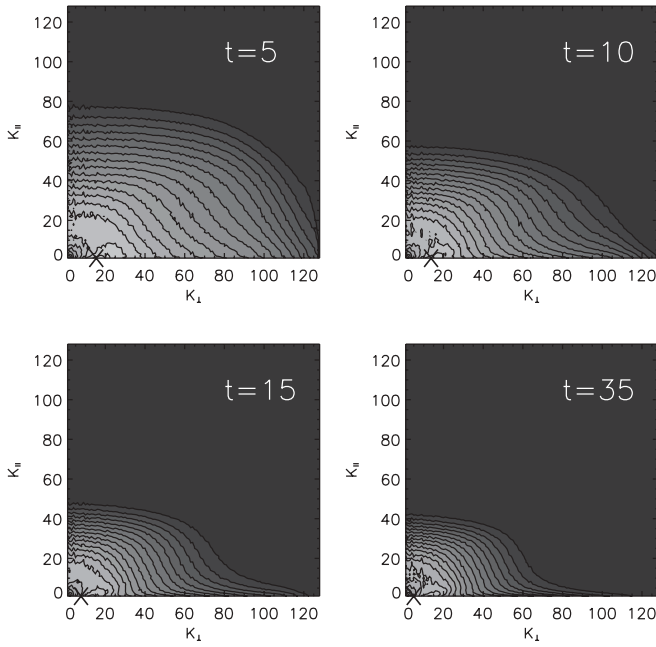
FIG. 12. Axisymmetric energy spectrum $e(k_\parallel, k_\perp)/\sin\theta$ at different times in run D. As in run B, the spectral energy distribution is anisotropic. The cross indicates the maximum of the spectrum at the different times.

of the energy is isotropic, in these figures the axisymmetric energy spectrum is divided by $\sin\theta$, where $\theta = \arctan(k_\parallel/k_\perp)$.

In the absence of rotation (Fig. 11), the spectrum shows an isotropic energy distribution evidenced by circular contour levels which maintain their shape as the flow decays. However,
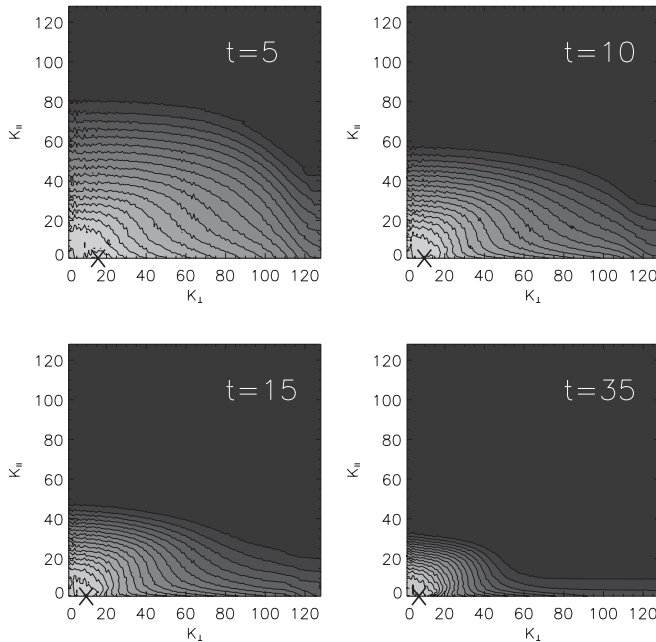

FIG. 13. Axisymmetric energy spectrum $e(k_\parallel, k_\perp)/\sin\theta$ at different times in run B. For rotating flows, the spectral distribution of energy becomes anisotropic with more energy near the $k_\parallel = 0$ plane. The cross indicates the maximum of the spectrum at the different times.
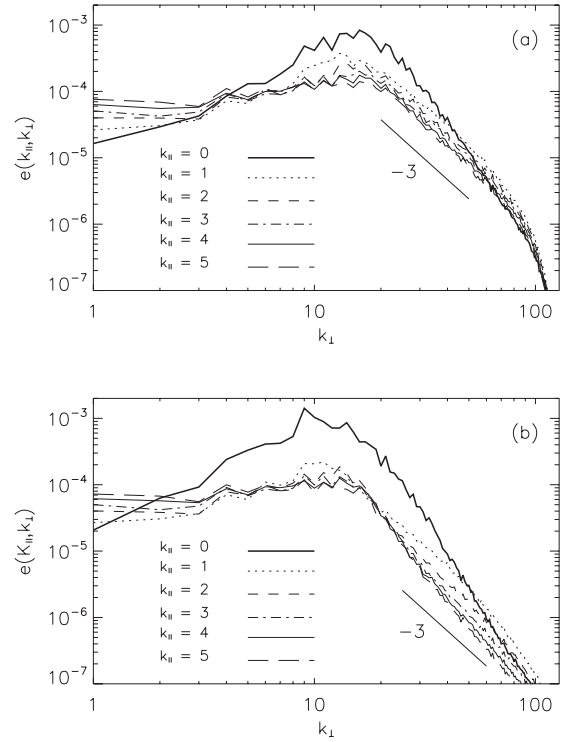

FIG. 14. Axisymmetric energy spectrum $e(k_\parallel, k_\perp)$ for run B for different values of $k_\parallel$ at (a) $t = 5$ and (b) $t = 10$. A $k_\perp^{-3}$ slope is shown as a reference.

when rotation is present, the spectral distribution of the energy becomes anisotropic with more energy near the $k_\parallel = 0$ axis (see Figs. 12 and 13). Already at $t = 10$, the maximum of the axisymmetric energy spectrum takes place in the $k_\parallel = 0$ axis, in agreement with the preferential transfer from 3D modes towards slow 2D modes observed at early times in the flux in Fig. 10 (as a matter of fact, the maximum of the spectrum is already located in the $k_\parallel = 0$ axis for times as early as $t = 5$).

After $t = 10$, the exchange of energy between 2D and 3D modes becomes negligible. As already observed in the time evolution of E_{2D} and E_{3D}, the energy in the 3D modes decays faster than the energy in 2D modes. This results in an increase of the spectral anisotropy as time evolves, with most of the energy near the $k_\parallel = 0$ axis at late times. At the same time, the peak of the spectrum slowly moves through the $k_\parallel = 0$ axis towards smaller values of $k_\perp$, although even at late times the peak is sufficiently far from $k_\perp = 1$.

The shape of the spectrum near the $k_\parallel = 0$ plane is of interest for many theories of homogeneous rotating turbulence (see, e.g., [11,48]). It is important to note that here the domain with finite size results in a discrete set of values for $k_\parallel$ so the $k_\parallel \to 0$ limit can not be studied, unlike homogeneous flows in infinite domains for which $k_\parallel$ is a continuum. Bearing in mind this limitation, we show in Figs. 14 and 15 the axisymmetric energy spectrum $e(k_\parallel, k_\perp)$ for fixed values of $k_\parallel$ (from 0 to 5), for runs B and D at two different times ($t = 5$ and 10).

Figures 14 and 15 confirm that most of the energy is contained in modes with $k_\parallel = 0$ (2D modes), and that the wave number $k_\perp$ at which the peak of the spectrum takes place slowly decreases with time (although the wave number is larger than $k_\perp = 1$). As an example, in run B the peak of
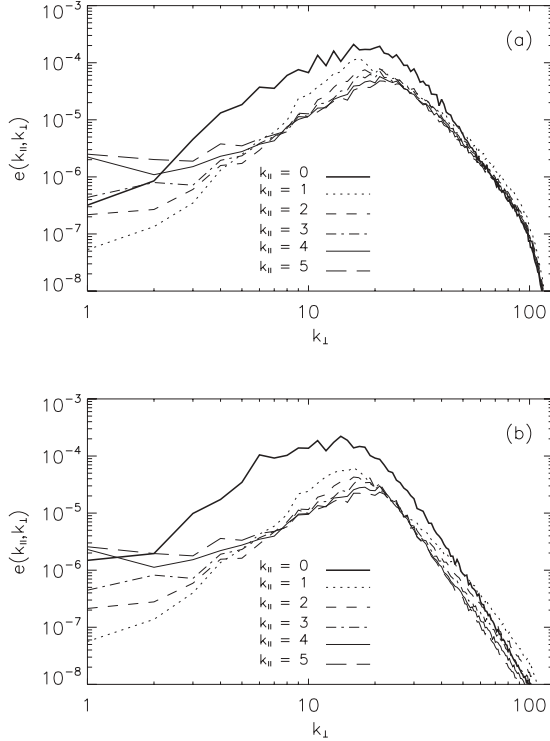
FIG. 15. Axisymmetric energy spectra $e(k_\parallel, k_\perp)$ for run D for different values of $k_\parallel$, at (a) $t = 5$ and (b) $t = 10$.

the spectrum for $k_\parallel = 0$ is at $k_\perp \approx 20$ at $t = 5$, at $k_\perp \approx 15$ at $t = 10$, and at $k_\perp \approx 8$ at $t = 35$. The spectrum for modes with $k_\parallel = 0$ also shows a positive slope for wave numbers smaller than the energy containing wave number, and the slope seems to be approximately preserved as the system evolves in time.

The spectra $e(k_\parallel, k_\perp)$ for $k_\parallel \geqslant 1$ are approximately flat for small wave numbers (especially for run B), and show a slope compatible with a $k_\perp^{-3}$ power law (especially for early times, at $t = 5$, and for the spectrum corresponding to $k_\parallel = 1$). This is consistent with the scaling $e(k_\parallel, k_\perp) \sim k_\parallel^{-1/2} k_\perp^{-3}$ valid for $k_\parallel / k_\perp \ll 1$ derived from inertial wave turbulence equations in Ref. [48], and also observed before in numerical simulations in Ref. [30].

V. CONCLUSIONS

We have analyzed numerical simulations of freely decaying rotating turbulence in periodic domains in the regime of intermediate Rossby number (Ro ≈ 0.1), with initial energy spectra $\sim k^2$ and $\sim k^4$. We first presented a brief theoretical discussion of conserved integral quantities for rotating turbulence using a von Kármán–Howarth equation which includes the Coriolis term due to rotation, extending previously derived results for Saffman turbulence [12], considering also the Batchelor spectrum. Assuming 2D and 3D modes are only weakly coupled in rotating turbulence, constancy of the anisotropic integral quantities $L_\perp$ or $I_\perp$ was used to derive phenomenologically the energy decay rate expected for energy in 2D modes.

In simulations without rotation, we recovered well known results for isotropic $\sim k^2$ and $\sim k^4$ turbulence, and also verified the approximate constancy of the isotropic integrals L and I. On the other hand, in the simulations with rotation, a self-similar decay was difficult to identify for the total energy, while L and I were found to grow rapidly during the entire decay. However, the decay of energy in two- and three-dimensional modes followed distinct power laws, in agreement with the phenomenological predictions and with constancy of $L_\perp$ and $I_\perp$, which were also observed to remain approximately constant in the simulations.

The separate power laws followed by $E_{2D}(t)$ and $E_{3D}(t)$ in decaying rotating turbulence require the interchange of energy between slow and fast modes to be negligible. We verified that this was the case by studying the flux of energy across planes with normal k_z in Fourier space. The results showed that energy is initially transferred from 3D to 2D modes, as expected for rotating turbulence at intermediate Rossby number [25], but that later the flux of energy between 3D and 2D modes becomes negligible. Contour levels of the axisymmetric energy spectral distribution show that in presence of rotation, the energy accumulates rapidly near the $k_\parallel = 0$ plane, and that at later times the anisotropy increases as a result of the different decay rates of the E_{2D} and E_{3D} components of the total energy.

Altogether, the results show that rotating turbulence is indeed affected by initial large-scale correlations in the flow, as different decay laws arise for $\sim k^2$ and $\sim k^4$ initial spectra.

[1] W. K. George, Phys. Fluids A **4**, 1492 (1992).

[2] P. A. Krogstad and P. A. Davidson, J. Fluid Mech. **680**, 417 (2011).

[3] T. Ishida, P. A. Davidson, and Y. Kaneda, J. Fluid Mech. **564**, 455 (2006).

[4] G. K. Batchelor and I. Proudman, Philos. Trans. R. Soc., A **248**, 369 (1956).

[5] P. G. Saffman, J. Fluid Mech. **27**, 581 (1967).

[6] P. G. Saffman, Phys. Fluids **10**, 1349 (1967).

[7] P. A. Davidson, J. Fluid Mech. **632**, 329 (2009).

[8] L. D. Landau and E. M. Lifshitz, *Fluid Mechanics*, 1st ed. (Pergamon, New York, 1959).

[9] C. Cambon and L. Jacquin, J. Fluid Mech. **202**, 295 (1989).

[10] C. Cambon, N. N. Mansour, and F. S. Godeferd, J. Fluid Mech. **337**, 303 (1997).

[11] F. Bellet, F. S. Godeferd, J. F. Scott, and C. Cambon, J. Fluid Mech. **562**, 83 (2006).

[12] P. A. Davidson, J. Fluid Mech. **663**, 268 (2010).

[13] N. Okamoto, P. A. Davidson, and Y. Kaneda, J. Fluid Mech. **651**, 295 (2010).

[14] L. Jacquin, O. Leuchter, C. Cambon, and J. Mathieu, J. Fluid Mech. **220**, 1 (1990).

[15] L. J. A. van Bokhoven, H. J. H. Clercx, G. J. F. van Heijst, and R. R. Trieling, Phys. Fluids **21**, 096601 (2009).

[16] C. Lamriben, P.-P. Cortet, and F. Moisy, Phys. Rev. Lett. **107**, 024503 (2011).

[17] P. J. Staplehurst, P. A. Davidson, and S. B. DalEziel, J. Fluid Mech. **598**, 81 (2008).

[18] C. N. Baroud, B. B. Plapp, H. L. Swinney, and Zhen-Su She, Phys. Fluids **15**, 2091 (2003).

[19] C. Morize and F. Moisy, Phys. Fluids **18**, 065107 (2006).

[20] F. Moisy, C. Morize, M. Rabaud, and J. Sommeria, J. Fluid Mech. **666**, 5 (2011).

[21] X. Yang and J. A. Domaradzki, Phys. Fluids **16**, 4088 (2004).

[22] W. C. Müller and M. Thiele, Europhys. Lett. **77**, 34003 (2007).

[23] L. J. A. van Bokhoven, C. Cambon, L. Liechtenstein, F. S. Godeferd, and H. J. H. Clercx, J. Turbulence **9**, 1 (2008).

[24] T. Teitelbaum and P. D. Mininni, Phys. Rev. Lett. **103**, 014501 (2009).

[25] L. Bourouiba and P. Bartello, J. Fluid Mech. **587**, 161 (2007).

[26] T. Teitelbaum and P. D. Mininni, Phys. Scr., T **142**, 014003 (2010).

[27] T. Teitelbaum and P. D. Mininni, Phys. Fluids **23**, 065105 (2011).

[28] K. D. Squires, J. R. Chasnov, N. N. Mansour, and C. Cambon, *Proceedings of the 74th Fluid Dynamics Symposium on Application of Direct and Large Eddy Simulation to Transition and Turbulence, Chania, Crete, Greece*, AGARD–CP–551, 1994.

[29] L. Bourouiba, D. N. Straub, and M. L. Waite, J. Fluid Mech. **690**, 129 (2012).

[30] M. Thiele and W.-C. Müller, J. Fluid Mech. **637**, 425 (2009).

[31] P. A. Davidson, *Turbulence: An Introduction for Scientists and Engineers* (Oxford University Press, Oxford, UK, 2004).

[32] A. N. Kolmogorov, Dokl. Akad. Nauk SSSR **31**, 538 (1941).

[33] P. S. Iroshnikov, Soviet Astronomy **7**, 566 (1963).

[34] R. H. Kraichnan, Phys. Fluids **8**, 1385 (1965).

[35] P. D. Mininni, A. Alexakis, and A. Pouquet, Phys. Fluids **21**, 015108 (2009).

[36] S. Fox and P. A. Davidson, Phys. Fluids **21**, 125102 (2009).

[37] L. M. Smith and Y. Lee, J. Fluid Mech. **535**, 111 (2005).

[38] J. Baerenzung, H. Politano, Y. Ponty, and A. Pouquet, Phys. Rev. E **77**, 046303 (2008).

[39] J. Baerenzung, P. D. Mininni, A. Pouquet, H. Politano, and Y. Ponty, Phys. Fluids **22**, 025104 (2010).

[40] J. Baerenzung, D. Rosenberg, P. D. Mininni, and A. Pouquet, J. Atmos. Sci. **68**, 2757 (2011).

[41] D. O. Gómez, P. D. Mininni, and P. Dmitruk, Adv. Space Res. **35**, 899 (2005).

[42] A. Craya, P. S. T. Ministère de l'Air **345** (1958).

[43] J. R. Herring, Phys. Fluids **17**, 859 (1974).

[44] J. Lee, Phys. Fluids **22**, 40 (1979).

[45] C. Cambon, C. Teesside, and D. Jeandel, J. Mech. Theor. Appl. **4**, 629 (1985).

[46] P. D. Mininni, D. Rosenberg, and A. Pouquet, J. Fluid Mech. **699**, 263 (2012).

[47] P. D. Mininni, Annu. Rev. Fluid Mech. **43**, 377 (2011).

[48] C. Cambon, R. Rubinstein, and F. Godeferd, New J. Phys. **6**, 73 (2004).